JACS Au
AN OPEN ACCESS JOURNAL OF THE AMERICAN CHEMICAL SOCIETY

pubs.acs.org/jacsau
Methods/Protocols

Quantitative Electrochemical Analysis Method for Cu Impurities in Nickel−Cobalt−Manganese Cathode Materials

Woo Yeoul Shim, Sangwoo Kim, JungHye Won, Cheol-Hee Park,* and Taek Dong Chung*

Cite This: JACS Au 2025, 5, 1060−1068

Read Online

ACCESS | Metrics & More | Article Recommendations | Supporting Information

ABSTRACT: Lithium-ion batteries are among the most important energy-storage devices. In this regard, nickel−cobalt−manganese (NCM) cathodes are widely used because of their high energy density and stability. Cu on NCM can enhance the overall performance by aiding lithium-ion transport through cation mixing; however, it leads to issues, such as internal short circuits. The precipitation pH of Cu is high, making its chemical separation from the NCM challenging. Given the impacts and the challenge of separation, an accurate quantification of the residual Cu content in the NCM cathode is essential. Inductively coupled plasma methods struggle with the accurate quantification of trace impurities in NCM owing to the high contents of material elements, leading to instrument malfunction and time-consuming labor. In this study, the introduction of electrochemical methods significantly weakened the matrix effect and facilitated the pretreatment of the solution. In particular, a thin-film electrode (TFE) made of Rh allowed quantification of the Cu present in commercial NCM powder. Cyclic voltammetry and an electrochemical quartz crystal microbalance were used to confirm the formation of two types of underpotential deposition (UPD) Cu on the Rh TFE. Square-wave voltammetry was used to analyze the kinetic differences in Cu_{upd} and quantify trace amounts of Cu with high sensitivity. The results included a relative standard deviation of 2.54%, linear range of 13−450 ppb, and limit of detection of 3.9 ppb. The method was successfully applied to commercial NCM products, where the standard addition method determined Cu content in the range 40−60 ppb. This method provides standardized guidelines for both laboratory and industry for evaluating the effects of impurities across various NCM cathodes.

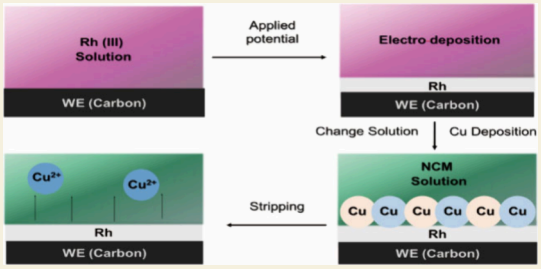

KEYWORDS: *Lithium-ion battery, NCM cathode, Copper (Cu), Thin film electrode, Underpotential deposition, Anodic stripping voltammetry*

INTRODUCTION

The global electric vehicle (EV) market is growing at an unprecedented rate, and lithium-ion batteries (LIBs) play an essential role in this transition. In 2023, the worldwide fleet of EVs, including plug-in hybrids and battery-electric vehicles (BEVs), surged to 14.2 million—a remarkable increase reflecting increasing consumer and regulatory support for ecofriendly transportation options.[1] The LIB technology is crucial because it determines the energy-storage capacity, efficiency, and overall cost-effectiveness of EVs.

Nickel-rich cathodes, particularly nickel−cobalt-manganese (NCM) and nickel−cobalt−aluminum (NCA) cathodes, play a crucial role in extending the driving range of electric vehicles due to their high energy density.[2] However, the challenge of securing cobalt (Co) has led to active research focused on increasing the nickel (Ni) content to reduce Co dependency, with careful consideration needed to maintain stability, safety, and lifespan. These advancements offer improved cost efficiency[3] and energy density, enhancing the competitiveness of lithium-ion batteries (LIBs) in the EV market.[4] Consequently, the development of high-Ni NCM cathodes with reduced Co content has accelerated.[5]

Another approach for reducing the Co content in NCM is the use of alternative dopants such as Al,[6−9] Fe,[10,11] and Cu,[11−13] which can enhance the rate capability and improve thermal stability. Recently, it has been recognized that the presence of a certain amount of Cu in the NCM cathode material not only improves the rate performance and discharge capacity but also enhances the stability through cation mixing with NCM in the transition metal layers.[14] However, excessive Cu can degrade the overall LIB performance and cause internal short circuits during charge and discharge, where Cu^{2+} deposited on the anode and cathode surfaces finally breaks through the separator, resulting in electrical contact between them.[15−18] Despite the significant impact on the overall battery performance, it is difficult to adjust the Cu content on the NCM cathode. The chemical separation of Cu from an NCM

Received: November 30, 2024
Revised: January 22, 2025
Accepted: January 23, 2025
Published: February 3, 2025

solution by adjusting the pH is more difficult than that of Al and Fe. This is because Al and Fe precipitate at relatively low pH owing to their low solubility products, whereas Cu precipitates at a pH similar to that for Ni, Co, and Mn, which are present in excess in NCM cathode materials, making complete separation difficult.[19]

Techniques used to measure the Cu content in NCM cathode materials include inductively coupled plasma (ICP) based methods,[12−14,22] energy-dispersive X-ray spectroscopy,[12−14] and atomic absorption spectroscopy (AAS).[20,21] However, these methods have been limited to detecting Cu at the percent scale or ppm levels and rarely achieve detection at sub-ppb levels. Although the most widely used ICP techniques are theoretically capable of detecting Cu at parts per billion levels, a high content of the NCM ions often causes instrument malfunction, making accurate measurements without extensive sample pretreatment challenging. According to the Pourbaix diagram, the redox potential of Cu is significantly higher than those of Ni, Co, and Mn, which allows for the selective deposition of Cu onto the electrode through the precise control of the applied voltage of the potentiostat. Using anodic stripping voltammetry (ASV), which is a well-established electrochemical trace analysis method, the solution was stirred to enhance the mass transport of Cu ions. This approach allowed the detection of Cu at sub-ppb levels and proved to be a highly sensitive and selective method for the analysis of trace Cu in complex cathode materials.

The application of ASV in battery research has been limited primarily because of the extensive adaptations and optimizations necessary for the accurate trace analysis of complex cathode materials such as NCM. Trace element analysis often relies on neutral or mildly acidic buffered solutions to stabilize electrochemical reaction rates on the electrode surface and ensure the chemical stability of the analyte. However, NCM cathode materials contain high contents of ions (e.g., NCM and Li), which, as previously mentioned, readily precipitate at pH > 3.5, necessitating the use of a strongly acidic environment for accurate quantification.[23] This requirement emphasizes the need for a specialized, optimized protocol that enables trace element analysis under acidic conditions without interference.

Thin-film electrodes (TFEs), particularly Hg TFE[24−29] and Bi TFE,[30−32] have historically been used in ASV. However, Hg is highly toxic, while the Bi signal overlaps with the Cu signal. Because there is a correlation between the two peaks, quantitative analysis is difficult.[32−34] The addition of Ga[35,36] and H_2O_2[37,38] eliminates the interaction between the Bi and Cu current peaks, but it is unknown how the introduction of additives affects the sample. Therefore, electrode materials that can detect Cu in addition to Hg and Bi, such as Te,[39,40] Se,[41] Sn,[42] Sb,[43] and Pd/Al,[44] were being actively explored.

This paper introduces a refined protocol for Cu quantification in NCM cathodes using ASV to address the challenges posed by high-ion-content environments. The methodology includes optimizing the acidic solution to dissolve Cu effectively, implementing sample pretreatment, and utilizing a new candidate—a robust Rh TFE resistant to acid and oxide-layer interference—for Cu detection. Additionally, we optimized the electrochemical parameters, such as those used in square-wave voltammetry (SWV), to increase the signal sensitivity under acidic conditions. By establishing these critical parameters, we lay a foundation for the accurate and reproducible analysis of trace elements in NCM, expanding the applicability of ASV in the field of battery research and beyond.

METHODS

Reagents

Nitric acid (68−70%) was purchased from SAMCHUN. Sodium nitrate (≥99.0%), sodium hydroxide (≥97.0%), aluminum(III) nitrate nonahydrate (99.997%), zinc(II) nitrate hexahydrate (≥99.0%), chromium(III) nitrate nonahydrate (≥99.0%), a Cu standard for AAS (1 g/L), and a Rh standard for AAS (1 g/L) were purchased from Sigma−Aldrich. Water was purified using a Milli-Q water purification system (Millipore, Billerica, MA, USA) for dilution and sample preparation. Nickel(II) nitrate hexahydrate (99.9985%) and cobalt(II) nitrate hexahydrate (99.999%) were purchased from Alfa Aesar. Manganese(II) nitrate hydrate (99.999%), lithium nitrate anhydrous (99.999%), and iron(III) nitrate nonahydrate (≥98.0%), were purchased from Thermo Scientific.

Preparation of NCM Cathode Solution

The NCM model solution was prepared by dissolving 10.74 g of nickel nitrate hexahydrate, 674 mg of cobalt nitrate hexahydrate, 1099 mg of manganese nitrate hydrate, 3.86 mg of lithium nitrate, 1.37 g of aluminum nitrate nonahydrate, 0.9 mg of zinc nitrate hexahydrate, 1.51 mg of chromium nitrate nonahydrate, and 1.42 mg of iron nitrate nonahydrate in 8 mL of a 0.1 M electrolyte solution. A liter of electrolyte was prepared by dissolving 8.5 g of sodium nitrate in a diluted nitric acid solution comprising a mixture of distilled water and nitric acid (ratio of 3:7, pH of approximately −0.35).

The NCM battery sample solution was prepared by dissolving 10 g of NCM cathode powder given by LG Energy Solution Co. (high Ni NCM with 90:5:5 ratio in 50 mL of a diluted nitric acid solution), followed by stirring for 2−3 h at 300 rpm. The sample solution was centrifuged at 7000 rpm for 5 min, followed by filtering with a 0.45 μm poly(tetrafluoroethylene) (PTFE) syringe filter. NaOH (2 g) was added, and NaOH solution (0.4 g/mL) was added dropwise until an overall solution pH of 2 was attained, followed by stirring at 1000 rpm for 2−3 h and centrifugation at 7000 rpm for 5 min. The supernatant was used for subsequent experiments.

Preparation of Rh TFE

A glassy carbon electrode (GCE, BAS) was initially polished with alumina powder (PK-4, BAS). Alumina powder (0.3, 0.05 μm) was mixed with distilled water, and 2 or 3 drops of this mixture were applied to the polishing pad. The electrode was then rotated clockwise and counterclockwise 50 times on the pad. After being polished, the electrode was sonicated for 1 min to remove residual particles. The GCE used as the working electrode (WE), Ag/AgCl as the reference electrode (RE), and Pt as the counter electrode (CE) were mounted on a homemade voltammetric cell with a Teflon cap (Figure 1). The hole diameters of the electrodes at the Teflon cap were 6.4, 1.0, and 6.0 mm for WE, CE, and RE, respectively. The WE was held in place by using a rubber ring.

To remove metal impurities from the surface, the CE was dipped in and out of a piranha solution for 5 s. (**Caution**: Piranha solution reacts violently with organic matter and should be handled with extreme care!) A Rh TFE was prepared by electrodepositing Rh onto the WE using a 0.5 g/L Rh solution, which was prepared by diluting a 1 g/L Rh AAS

https://doi.org/10.1021/jacsau.4c01159
JACS Au 2025, 5, 1060−1068

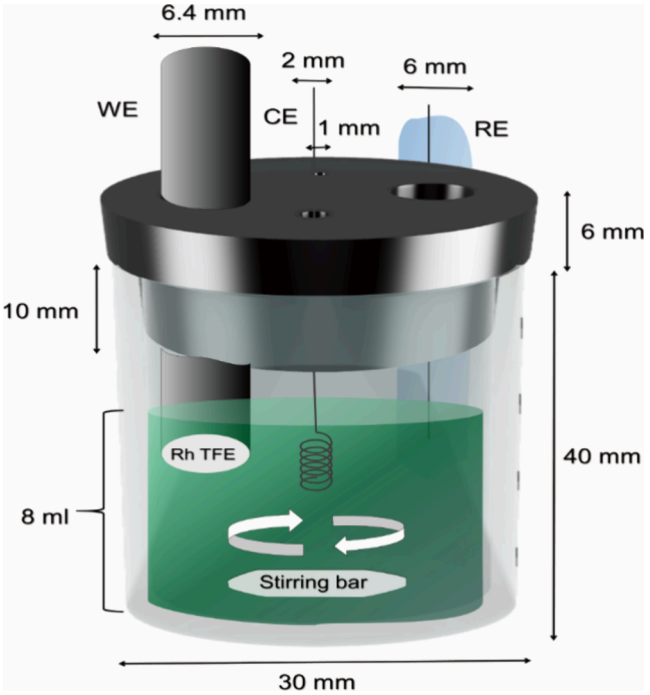

Figure 1. A glass cell and Teflon cap designed for the electrochemical quantification of Cu in the NCM cathode solution. The thickness of the glass wall is 2 mm. The Teflon cap has a total of four holes, designed to accommodate a three-electrode system (WE for 6.4 mm, RE for 6 mm, and CE for 2 mm) and N_2 purging (1 mm) 8 mL of solution for an experiment.

standard solution with a supporting electrolyte. The solution was purged with nitrogen gas for 300 s to eliminate the initial dissolved oxygen. Rh plating was done via cyclic voltammetry (CV) (initial potential, 0.4 V; reversal potential, −0.3 V; cycles, 1; scan rate, 25 mV/s). The CV profiles were analyzed to check if the electrode was plated properly, and then, the set of electrodes was rinsed with water and blown with nitrogen gas.

Instruments

Cyclic voltammograms and square-wave voltammograms were obtained by using an Autolab potentiostat (PGSTAT302N, Nova 1.10, Metrohm) instrument. The WE was a GCE (3.0 mm diameter, Bioanalytical Systems, Inc., West Lafayette, Indiana 47906, USA) with a thin-film Rh. Electrode mass data were obtained by using an electrochemical quartz crystal microbalance (EQCM) and a CHI440 electrochemical workstation (CHI Instruments). A CHI 7.995 MHz QCM sensor (RenLux Crystal) was used as the WE. An Ag/AgCl RE with a Vycor tip and a Pt auxiliary electrode were used. A magnetic stirrer (Jeio Tech, MS-32M) and a stirring bar (Daihan Scientific MS-20, South Korea) provided convective transport during the dissolution of the NCM powder and electrochemistry experiments.

Electrochemical Analysis

Either 8 mL of the NCM model solution or 8 mL of the NCM battery sample solution was added to the electrochemical cell, followed by purging with nitrogen gas for 5 min. The deposition potential (−0.2 V) was applied for 5 min with stirring (1000 rpm), followed by 30 s without stirring, to obtain a quiescent solution. SWV was performed to measure the Cu stripping current signal (initial potential, −0.2 V; stop potential, 0.4 V; step potential, 10 mV; modulation amplitude, 75 mV; frequency, 90 Hz). Then, the stripping potential (0.4 V) was applied to eliminate the deposited Cu on the Rh TFE electrochemically for 180 s with stirring (1000 rpm) for restoring the Rh TFE surface to a clean, Cu-free state, followed by a period of 10 s without stirring to obtain a quiescent solution. Finally, the SWV protocol with parameters identical to those used for Cu detection was repeated to measure the background signal. The analysis was performed by using the current obtained by subtracting the current of the second SWV from that of the first SWV. The entire procedure was automated and controlled by Autolab software. For the standard addition method, a 10 mg/L Cu solution, which was prepared by diluting a 1 g/L Cu AAS standard solution with a supporting electrolyte solution, was added.

RESULTS AND DISCUSSION

To examine the redox behavior of Cu in a nitric acid solution, we performed CV on a GCE. At −0.6 V, three cathodic peak potentials (−0.07, −0.33, and −0.45 V) and one anodic peak potential (0.09 V) were observed (Figure 2).

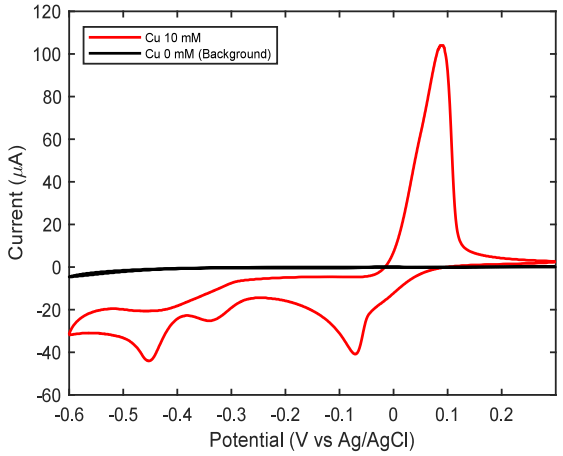

Figure 2. Cyclic voltammogram at 10 mM $Cu(NO_3)_2$ (red line) and 0 mM $Cu(NO_3)_2$ (black line) on 0.1 M $NaNO_3$ (pH 2.0) between −0.6 and 0.3 V at 25 mV/s.

When the counterion was changed from nitrate to sulfate, the reduction peak potentials corresponding to −0.33 and −0.45 V disappeared (Figure S1). This indicates that these two peaks are not due to the reduction of Cu ions but are related to the reduction of nitrate ions. The area of the anodic current at 0.09 V, where Cu was oxidized, was calculated by changing the cathodic reversal potential. The anodic charge increased linearly as the reversal potential was further decreased (Figure S2). This implies that the peaks related to nitrate hardly affect the reduction plating of Cu, because if the scan rate is constant, the reduction time for Cu increases linearly as the cathodic limit potential constantly increases. Nevertheless, the reduction potential for Cu analysis was determined to be −0.2 V to exclude the potential impact of the reduction of nitrate ions.

To verify the successful Rh plating of the GCE, CV and electrochemical impedance spectroscopy (EIS) were performed in a 10 mM aqueous solution of nitric acid (Figure 3).

Rh—a Pt-like metal—exhibits a distinct current signal under acidic conditions, such as those in hydrogen adsorption or the hydrogen evolution reaction. At elevated potentials, the

https://doi.org/10.1021/jacsau.4c01159
JACS Au 2025, 5, 1060−1068

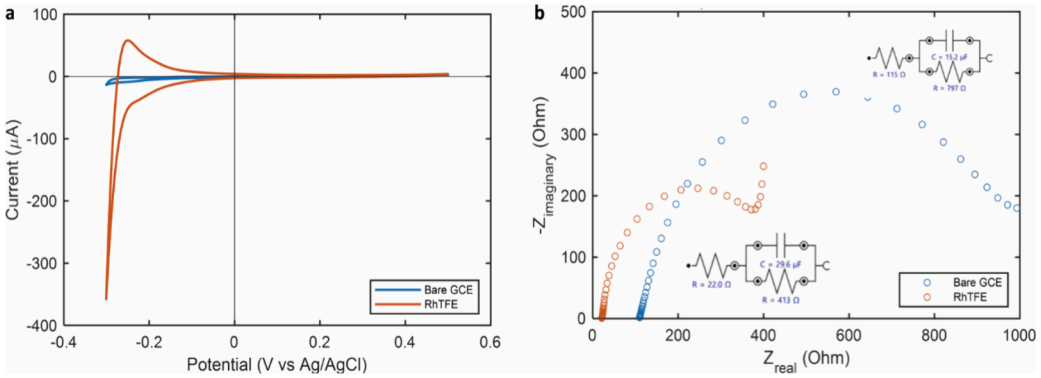

Figure 3. (a) Comparison between cyclic voltammogram of 0.1 M $NaNO_3$ (pH 2.0) at GCE and Rh TFE between −0.3 and 0.5 V at 25 mV/s. (b) Comparison between Nyquist plot measured at a constant potential −0.2 V with V_{rms} of 10 mV and a frequency range of 1−100 kHz (fitted by NOVA 2.1.3).

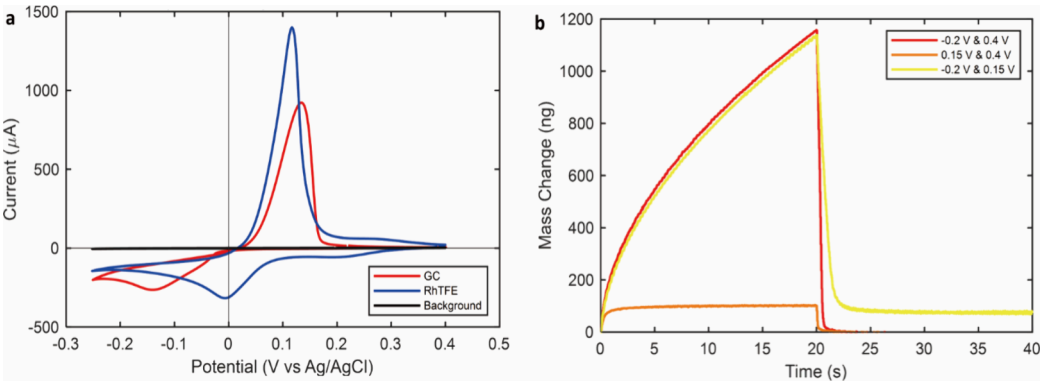

Figure 4. (a) Cyclic voltammogram at GCE (red line) and Rh TFE (blue line) of 10 mM $Cu(NO_3)_2$ on NCM model solution between −0.25 and 0.4 V at 25 mV/s. (b) EQCM mass change of Rh TFE of diluted 0.5 g/L Cu AAS standard solution. A specific voltage was applied for 20 s, followed by a different voltage for another 20 s. Initially, the red and yellow lines were subjected to −0.2 V, while the orange line was subjected to 0.15 V. Subsequently, the red and orange lines were subjected to 0.4 V, and the yellow line was subjected to −0.15 V.

currents associated with the rhodium oxide formation and reduction became apparent. Notably, no current attributable to Rh oxidation was observed until the potential reached 0.5 V. In contrast, the GCE did not generate discernible faradic currents. This observation underscores the unique electrochemical behavior of the Rh TFE. The EIS Nyquist plot was fitted with an R(RC) equivalent circuit model composed of a parallel circuit of charge-transfer and double-layer capacitance in series with the solution resistance. The analysis revealed that the charge-transfer resistance of the Rh TFE decreased from 797 to 413 Ω. Concurrently, the double-layer capacitance increased from 15.2 to 29.6 μF. These observations suggest that the Rh plating increased the electron transfer rate and the effective surface area of the electrode.

In Figure 4, the redox behavior of Cu in Rh TFE exhibits a notable shift in the reduction peak potential from −0.15 to 0 V (Figure 4a). This shift indicates the thermodynamically favorable reduction of Cu on Rh. Furthermore, a steeper increase in the anodic current suggests accelerated oxidation kinetics of Cu. In the potential window 0.2−0.3 V, a distinct pair of redox peaks is observed for the Rh TFE, which is absent in the case of the bare GCE and represents a separate redox process distinct from the general bulk deposition of Cu. This was corroborated by CV conducted with the cathodic reversal potential set as 0.15 V, which revealed an additional shoulder peak (Figure S3). The appearance of peaks different from the original redox peaks indicated that a distinct form of the redox reaction occurred on the Rh substrate.

For further analysis, the mass change of the electrode was monitored using the EQCM. Upon application of −0.2 V, the weight increased continuously. However, when 0.15 V was applied, it remained constant, indicating no further changes (Figure 4b). From the CV and EQCM data, it is evident that underpotential deposition (UPD) occurs in conjunction with three-dimensional bulk deposition when Cu is plated on Rh. This observation aligns with the findings of previous studies.[45−47] In contrast to bulk deposition, the UPD occurred only in a few monolayers on Rh. Therefore, it is not surprising that after a certain amount of Cu was plated on Rh via UPD, no further plating occurred. This is consistent with the observed cessation of the electrode weight change in the EQCM measurements.

To investigate the effect of the Cu_{upd} phenomenon on Rh, the changes in the electrode mass during the CV cycle were examined (Figure S4). When the anodic reversal potential was confined to 0.4 V to prevent the oxidation of Rh to rhodium oxide, the net mass change of the electrode from one cycle to the next was observed to be zero (red line). When the potential was increased to 0.8 V, a condition conducive to the production of rhodium oxide was observed: a consistent reduction in the weight of the electrode from cycle to cycle (orange line). This observation differs from the gradual increase in the electrode weight when CV was performed

https://doi.org/10.1021/jacsau.4c01159
JACS Au 2025, 5, 1060−1068

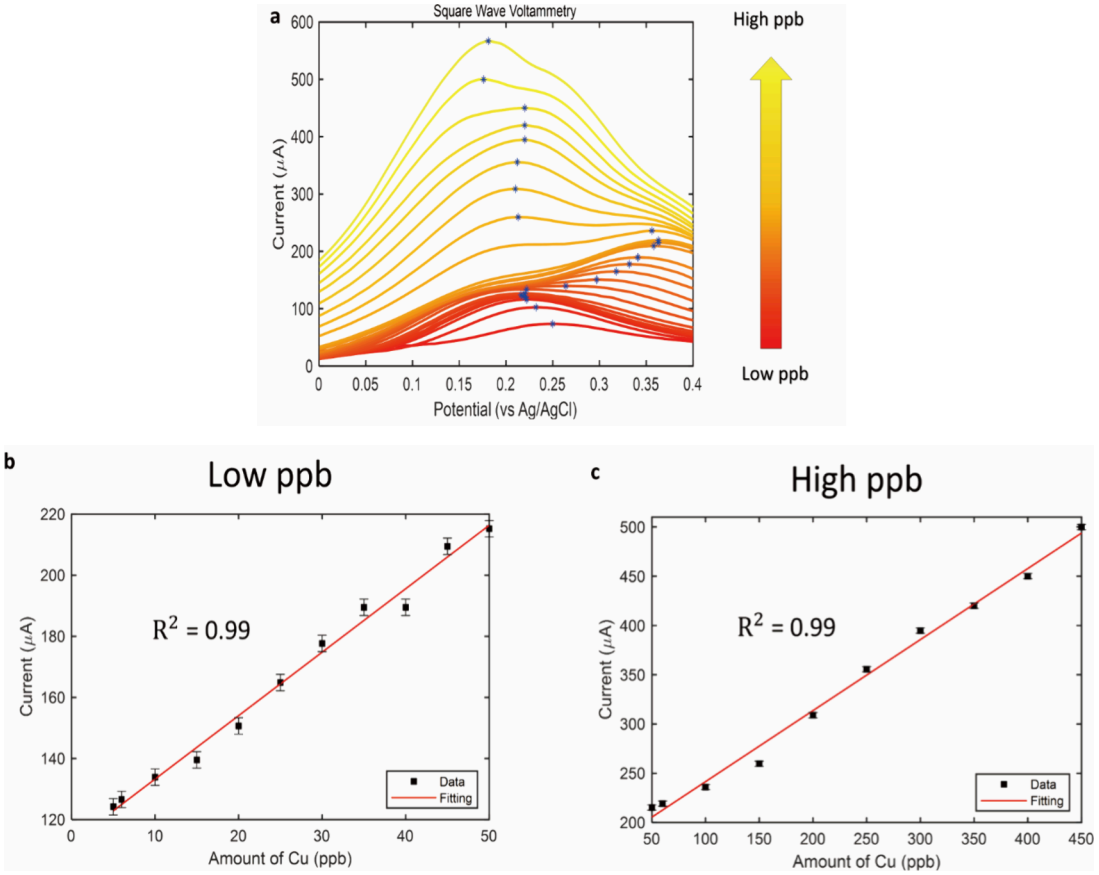

Figure 5. (a) Square wave voltammogram of different concentrations of Cu on NCM model solution between 0 and 0.4 V. The SWV parameters: modulation amplitude of 75 mV, step potential of 10 mV, and frequency of 90 Hz. Plots of amount of Cu (in ppb) versus SWV peak current (indicated by blue dots in Figure 5a) for (b) low and (c) high ppb.

using only a Cu-free electrolyte. These findings suggest that, by adjusting the oxidation potential to the level at which Rh is oxidized, Cu_{upd} facilitates the dissolution of Rh on the electrode, which can affect the reproducibility of the signal necessary for Cu trace analysis. To mitigate the aforementioned effect, the oxidation voltage was judiciously set at 0.4 V for further trace analysis.

Figure 5a shows the variation in the SWV current as a function of the Cu content in the NCM solution. Several experimental parameters were optimized to obtain the maximum SWV current signal (Figure S5). The relative standard deviation (RSD) was 2.54%, the linear dynamic range was 13−450 ppb, and the limit of detection (LOD) was 3.9 ppb, as calculated using standard deviation of the background signal and slope of the calibration curve. These performance characteristics can be considered comparable to those of Cu-ion selective electrode (ISE), but their pretreatments are complex and difficult to disregard the interference effects of high concentrations of NCM cathode solution.[48−50] Additionally, our approach, which leverages the characteristics of UPD, has a high potential for improved performance if the Cu deposition area can be increased, similar to the case for the use of nanoparticles. The peak current, when plotted as a function of the additional spiked Cu content (ppb), yielded two calibration curves. These curves exhibited high linearity (R^2 = 0.989 and 0.991, respectively) but different slopes. For a relatively low Cu content (<50 ppb), the slope was approximately 2.08 μA/ppb. For higher Cu contents (>50 ppb), the slope was smaller, i.e., approximately 0.74 μA/ppb (Figure 5b,c).

The behaviors of the peak current and peak potential varied at a Cu content of 50 ppb. For a lower content, the peak potential gradually increased to 0.35 V. In contrast, for higher contents (ppb), the potential remained relatively constant at approximately 0.22 V. The distinct behaviors of the peak current and potential suggest the generation of two types of Cu_{upd} on the Rh surface. To eliminate the possibility that one of these is bulk deposition, SWV was performed after depositing a high content of Cu whose peak potential was 0.12 V, indicating that the current signal in Figure 4a is related to UPD (Figure S6), not bulk deposited Cu.

Further confirmation of the distinct UPD behavior was obtained through an EQCM study. The UPD behavior when the plating voltage was set to 0.15 V differed from that when it was set to 0.1 or 0.05 V (Figure S7). Previous research has revealed two types of Cu_{upd} generated at different energy sites when Cu is electroplated on Rh. However, these peaks were observed at the potential at which rhodium oxide was generated.[46] Our findings suggest that two different types of Cu_{upd} can be generated even in the absence of a rhodium oxide layer.

Taking the logarithm of the Cu content (ppb), there was a consistent increase at peak potential with increasing log(ppb) in the low-content region, whereas it remained constant in the higher-content regions (Figure 6a, red arrow). In the low-content region, the trend of the SWV peak potential exhibited a high degree of linearity (R^2 = 0.976) (Figure 6b). If the

https://doi.org/10.1021/jacsau.4c01159
JACS Au 2025, 5, 1060−1068

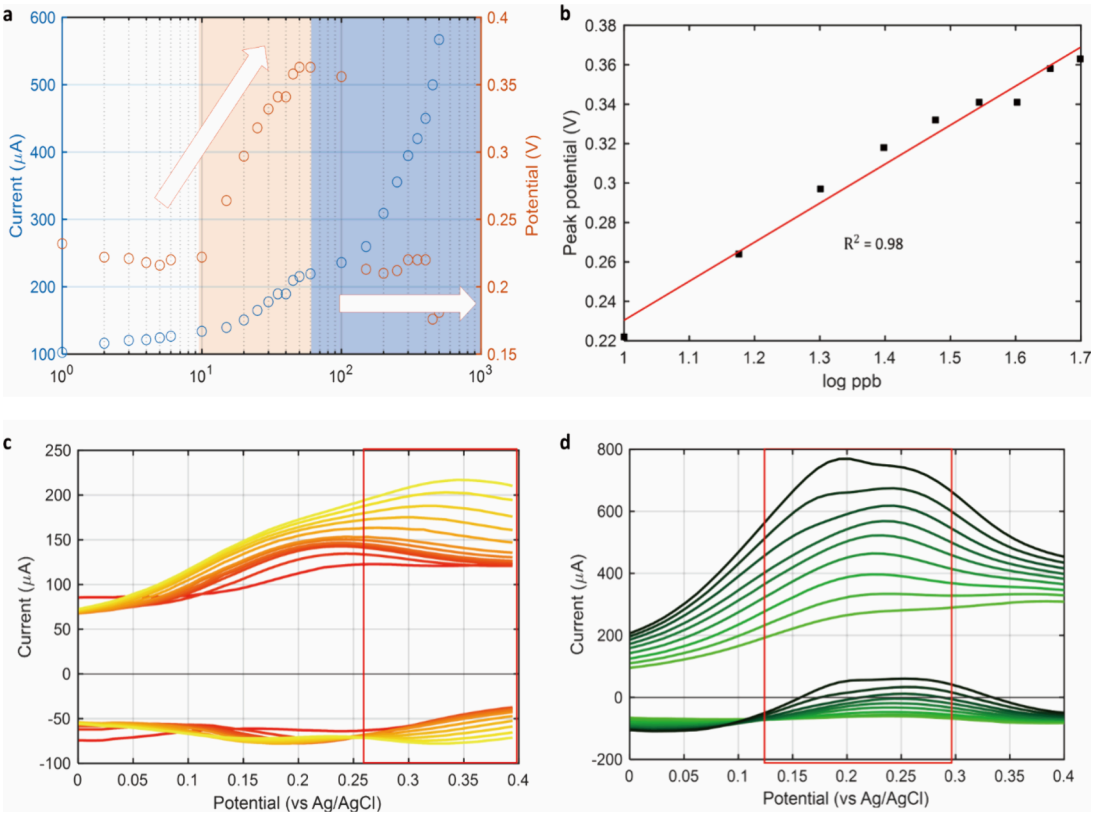

Figure 6. (a) A log[Cu^{2+}] versus SWV peak potential (red) and peak current plot (blue). (b) Linear fitting plot of log[Cu^{2+}] vs peak potential. (c, d) Forward current (upper part) and backward current (lower current) at low ppb (Cu ppb increases from red to yellow) and high ppb regions (Cu ppb increases from green to black), respectively.

electron transfer between Cu_{upd} and Cu^{2+} is rapid and electrochemically reversible, it adheres to the Nernst equation:

$$E = E^{0'} + \frac{RT}{nF} \ln \frac{[Cu^{2+}]}{[Cu_{upd}]} \approx E^{0'} + \frac{RT}{nF} \ln[Cu^{2+}]$$

(Cu_{upd} activity as 1)

Assuming the activity of Cu_{upd} to be 1, the redox potential increases proportionally to the logarithm of [Cu^{2+}]. Given the nature of the trace analysis, the amount of [Cu^{2+}] present in the bulk solution was minimal. Consequently, [Cu^{2+}] computed using the Nernst equation originates from the oxidation of Cu_{upd} that is situated sufficiently close to the electrode to be reduced again during the short pulse cycle of the SWV.

The variation in backward current in the SWV with respect to the amount of Cu in the low-parts per billion region was also examined. The backward current increased with the amount of Cu (Figure 6c). The potential pulse provided by the SWV oxidized Cu_{upd} in the forward step, and the oxidized Cu ions were subsequently reduced in the backward step. Therefore, an increase in the backward current signifies an increase in the amount of Cu^{2+} reduced near the electrode surface. Conversely, in the high parts per billion region, the backward current decreased progressively, and an oxidation current was observed (Figure 6d). This suggests that the pulse period was too short for Cu^{2+}, which was produced by the oxidation of Cu_{upd}, to be reduced. Strongly adsorbed Cu_{upd} in the low-ppb region, i.e., strongly adsorbed Cu_{upd}, which was oxidized at higher potentials, exhibited fast redox kinetics. Thus, as the amount of Cu increased, the overall degree of oxidation and reduction increased simultaneously, manifesting an electrochemically reversible Nernstian behavior. In contrast, Cu_{upd} in the high-ppb region, that is, weakly adsorbed Cu_{upd}, which is oxidized at a lower potential, exhibits slow redox kinetics, and the reduction of Cu^{2+} does not occur rapidly. Figure 7 shows the results of the standard addition method applied to a solution prepared by dissolving commercial NCM powder in nitric acid using an AAS standard solution. In each

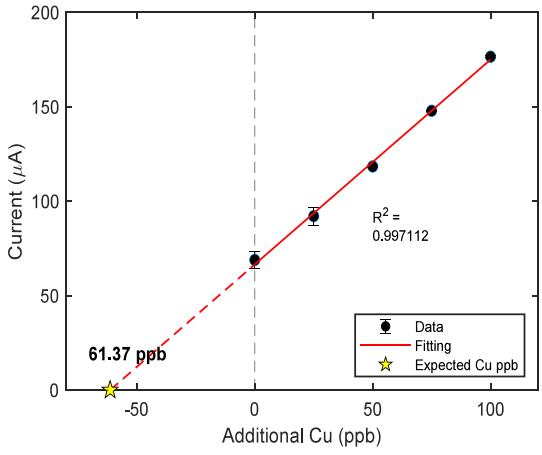

Figure 7. Calibration curve by standard addition method of the amount of Cu (ppb) versus SWV peak current. An estimated amount of Cu obtained through extrapolation is indicated by yellow stars. (n = 3−7).

https://doi.org/10.1021/jacsau.4c01159
JACS Au 2025, 5, 1060−1068

of 3−7 successive experiments, the signal was found to be reproducible with a high degree of precision, as indicated by an RSD of 6.8%. Weakly adsorbed Cu_{upd} was generated, and it exhibited a peak potential of 0.22 V (Figure S8).

A high degree of linearity (R^2 = 0.997) was observed between the amount of Cu and the peak current. By extrapolation of the *x*-intercept, the amount of Cu present in the battery was calculated to be 61.37 ppb. The same methodology was used for commercial cathode samples given by LG Energy Solution Co. The measurements obtained from these experiments are presented in Table 1.

Table 1. Measured Cu Average in ppb and Corresponding Standard Deviation (n = 3−7) at Several Commercial NCM Samples (BS1−BS6)

Battery Sample	Average (ppb)	Standard Deviation (ppb)
BS1	49.78	12.26
BS2	61.11	17.61
BS3	59.39	32.95
BS4	58.96	19.98
BS5	56.72	18.73
BS6	40.49	4.03

To investigate the effects of impurities other than the major NCM elements (Ni, Co, Mn, Li, and Al) and the analyte Cu, several possible impurities were spiked at parts per billion levels, and the standard addition method was used to compare the estimated Cu contents (Figure 8a). To investigate the effects of impurities other than the major NCM elements (Ni, Co, Mn, Li, and Al) and the analyte Cu, several possible impurities were spiked at ppb levels, and the standard addition method was used to compare the estimated Cu contents (Figure 8a). The types and amounts of impurities present in NCM cathode materials can vary depending on not only the doping elements used[51,52] but also wear caused by friction with metal equipment or accumulation due to repeated manufacturing environment of the cathode material. Therefore, we collaborated with LG Energy Solution, which manufactures battery-grade NCM cathode materials, and as a result of our discussions, Fe, Cr, and Zn were selected as target elements. When 5 ppb of Fe was added, the quantified Cu content remained virtually unchanged. Similarly, the addition of 100 ppb of Zn resulted in negligible variations in the measured Cu levels. In contrast, the addition of 50 ppb of Cr led to an increase of approximately 10 ppb in the predicted Cu content. However, when Fe, Cr, and Zn were introduced simultaneously, the Cu content was measured with a high accuracy within a margin of 10 ppb. Although the reason for the increase in the Cu content due to Cr requires further investigation, it is concluded that the combined presence of multiple elements mitigated the influence of Cr, resulting in a minimal overall impact on the estimated Cu content.

CONCLUSIONS

This study involved determining the optimal solution conditions for dissolving cathode material powders containing detectable levels of Cu impurities. We quantified parts per billion-level Cu impurities in battery cathode materials under strongly acidic solution conditions containing various ions using a Rh TFE. The two types of Cu_{upd} with different redox kinetics formed on the Rh TFE surface, analyzed through EQCM and SWV, have been identified as critical phenomena for detecting trace amounts of Cu. This finding suggests the possibility that other metals capable of inducing Cu_{upd} (e.g., Pt and Au) may also enable the detection of trace amounts of Cu, provided that the formation of oxide layers is avoided.

In addition, we developed a pretreatment protocol for electrochemical analysis, optimized the Rh TFE modification process, and fine-tuned the SWV parameters. We demonstrated the high accuracy (within tens of parts per billion), reproducibility (RSD: 2.54%), signal linearity (R^2 = 0.99), and good LOD (3.9 ppb) of the method using a model solution prepared with high-purity laboratory reagents. Moreover, the effects of various additional elements were evaluated to confirm that their presence did not significantly affect the accuracy of the proposed method when applied to commercial cathode powder. Additionally, commercial NCM cathode solutions exhibited high signal linearity in the standard addition method (R^2 = 0.997), confirming that several solution samples contained approximately 40−60 ppb Cu impurities.

This study lays the groundwork for developing an economical Cu detection methodology using carbon paste electrodes, which can allow efficient and straightforward quality control inspections of Cu impurities in NCM cathodes, even by novices, within commercial settings. Furthermore, this methodology can be extended to foreign metal adatom

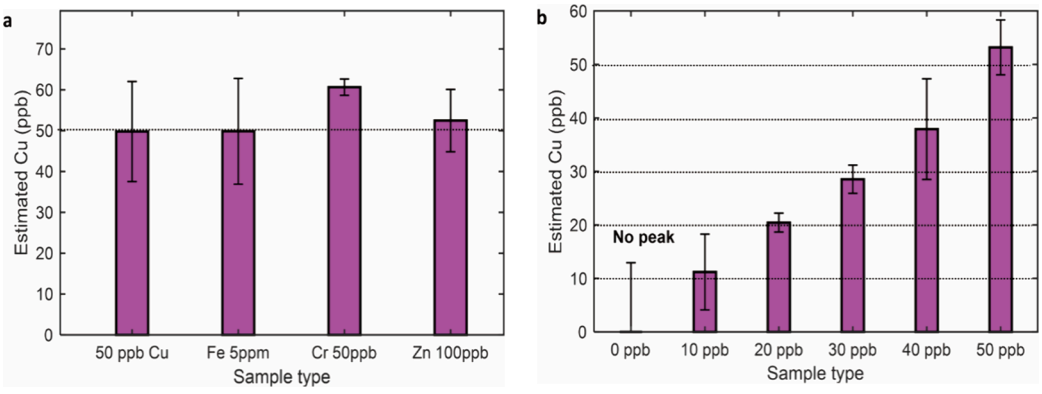

Figure 8. (a) Interference effect of Fe, Cr, and Zn. From left to right, a model solution with 50 ppb of Cu, a solution with 5 ppm of Fe added, a solution with 50 ppb of Cr added, and a solution with 100 ppb of Zn added, respectively. (b) Accuracy test at model solution with 0, 10, 20, 30, 40, 50 ppb Cu. (n = 3−7).

https://doi.org/10.1021/jacsau.4c01159
JACS Au 2025, 5, 1060−1068

catalysts, for example, to investigate the plating kinetics of UPD adatoms.

■ ASSOCIATED CONTENT

Supporting Information

The Supporting Information is available free of charge at https://pubs.acs.org/doi/10.1021/jacsau.4c01159.

CVs, relationship between anodic charge and reversal potential, discrimination of shoulder peaks by changing reversal potential, TFE mass change during cyclic voltammetry, optimization parameters, stripping current signal, EQCM mass change, square wave voltammogram (PDF)

■ AUTHOR INFORMATION

Corresponding Authors

Cheol-Hee Park − *Analytical Sciences Center, LG Energy Solution R&D Campus Daejeon, Daejeon 34122, Republic of Korea*; Email: pmoka@lgensol.com

Taek Dong Chung − *Department of Chemistry, Seoul National University, Seoul 08826, Republic of Korea; Advanced Institutes of Convergence Technology, Suwon-si 16229 Gyeonggi-do, Republic of Korea*; orcid.org/0000-0003-1092-8550; Email: tdchung@snu.ac.kr

Authors

Woo Yeoul Shim − *Department of Chemistry, Seoul National University, Seoul 08826, Republic of Korea*

Sangwoo Kim − *Analytical Sciences Center, LG Energy Solution R&D Campus Daejeon, Daejeon 34122, Republic of Korea*

JungHye Won − *Analytical Sciences Center, LG Energy Solution R&D Campus Daejeon, Daejeon 34122, Republic of Korea*

Complete contact information is available at: https://pubs.acs.org/10.1021/jacsau.4c01159

Author Contributions

CRediT: **Woo yeoul Shim** conceptualization, data curation, formal analysis, investigation, methodology, project administration, software, supervision, validation, visualization, writing - original draft, writing - review & editing; **Sangwoo Kim** project administration, resources, supervision, writing - review & editing; **JungHye Won** project administration, resources, supervision, writing - review & editing; **Cheol-Hee Park** project administration, resources, supervision, writing - review & editing; **Taek Dong Chung** conceptualization, methodology, project administration, resources, software, validation, writing - review & editing.

Notes

The authors declare no competing financial interest.

■ ACKNOWLEDGMENTS

This research was supported by the National Research Foundation of Korea (NRF) grant funded by the Korea government (MSIP) (No. RS-2021-NR060082 and No. RS-2022-NR070547).

■ ABBREVIATIONS

NCM, Nickel−Cobalt−Manganese; CV, Cyclic Voltammetry; EQCM, Electrochemical Quartz Crystal Microbalance; SWV, Square Wave Voltammetry; EIS, Electrochemical Impedance Spectroscopy; ASV, Anodic Stripping Voltammetry; GCE, Glassy Carbon Electrode; TFE, Thin Film Electrode; ICP, Inductively Coupled Plasma

■ REFERENCES

(1) Roland, I. Global EV Sales for 2023. *EV VOLUMES*, January 22, **2024**, https://ev-volumes.com/news/ev/global-ev-sales-for-2023/ (accessed 2024-11-28).

(2) Manthiram, A. A Reflection on Lithium-Ion Battery Cathode Chemistry. *Nat. Commun.* **2020**, *11* (1), 1550.

(3) Myung, S.-T.; Maglia, F.; Park, K.-J.; Yoon, C. S.; Lamp, P.; Kim, S.-J.; Sun, Y.-K. Nickel-Rich Layered Cathode Materials for Automotive Lithium-Ion Batteries: Achievements and Perspectives. *ACS Energy Lett.* **2017**, *2* (1), 196−223.

(4) Dunn, B.; Kamath, H.; Tarascon, J.-M. Electrical energy storage for the grid: a battery of Choice. *Science* **2011**, *334*, 928−935.

(5) Li, W.; Erickson, E. M.; Manthiram, A. High-Nickel Layered Oxide Cathodes for Lithium-Based Automotive Batteries. *Nat. Energy* **2020**, *5* (1), 26−34.

(6) You, Y.; Celio, H.; Li, J.; Dolocan, A.; Manthiram, A. Modified High-nickel Cathodes with Stable Surface Chemistry against Ambient Air for lithium-Ion Batteries. *Angew. Chem.* **2018**, *130* (22), 6590−6595.

(7) Delmas, C.; Saadoune, I.; Rougier, A. The Cycling Properties of the $Li_xNi_{1-y}Co_yO_2$ Electrode. *J. Power Sources* **1993**, *44* (1−3), 595−602.

(8) Ohzuku, T.; Ueda, A.; Kouguchi, M. Synthesis and Characterization of $LIAl_{1/4}Ni_{3/4}O_2$ (R3m) for Lithium-ion (Shuttlecock) Batteries. *J. Electrochem. Soc.* **1995**, *142* (12), 4033−4039.

(9) You, Y.; Celio, H.; Li, J.; Dolocan, A.; Manthiram, A. Modified High-nickel Cathodes with Stable Surface Chemistry against Ambient Air for lithium-Ion Batteries. *Angew. Chem. Inter. Ed.* **2018**, *57* (22), 6480−6485.

(10) Liu, D.; Wang, Z.; Chen, L. Comparison of Structure and Electrochemistry of Al- and Fe-Doped $LiNi_{1/3}Co_{1/3}Mn_{1/3}O_2$. *Electrochim. Acta* **2006**, *51* (20), 4199−4203.

(11) Nasser, O. A.; Petranikova, M. Review of Achieved Purities after Li-Ion Batteries Hydrometallurgical Treatment and Impurities Effects on the Cathode Performance. *Batteries* **2021**, *7* (3), 60.

(12) Wu, T.; Wang, G.; Liu, B.; Huang, Q.; Su, Y.; Wu, F.; Kelly, R. M. The Role of Cu Impurity on the Structure and Electrochemical Performance of Ni-Rich Cathode Material for Lithium-Ion Batteries. *J. Power Sources* **2021**, *494*, 229774.

(13) Do, M. P.; Jegan Roy, J.; Cao, B.; Srinivasan, M. Green Closed-Loop Cathode Regeneration from Spent NMC-Based Lithium-Ion Batteries through Bioleaching. *ACS Sustain. Chem. & Eng.* **2022**, *10* (8), 2634−2644.

(14) Zhang, R.; Meng, Z.; Ma, X.; Chen, M.; Chen, B.; Zheng, Y.; Yao, Z.; Vanaphuti, P.; Bong, S.; Yang, Z.; Wang, Y. Understanding Fundamental Effects of Cu Impurity in Different Forms for Recovered $LiNi_{0.6}Co_{0.2}Mn_{0.2}O_2$ Cathode Materials. *Nano Energy* **2020**, *78*, 105214.

(15) Huang, L.; Liu, L.; Lu, L.; Feng, X.; Han, X.; Li, W.; Zhang, M.; Li, D.; Liu, X.; Sauer, D. U.; Ouyang, M. A Review of the Internal Short Circuit Mechanism in Lithium-ion Batteries: Inducement, Detection and Prevention. *Int. J. Energy Res.* **2021**, *45* (11), 15797−15831.

(16) Zhang, G.; Wei, X.; Tang, X.; Zhu, J.; Chen, S.; Dai, H. Internal Short Circuit Mechanisms, Experimental Approaches and Detection Methods of Lithium-Ion Batteries for Electric Vehicles: A Review. *Renew. Sustain. Energy Rev.* **2021**, *141*, 110790.

(17) Sun, Y.; Yuan, Y.; Lu, L.; Han, X.; Kong, X.; Wang, H.; Ouyang, M.; Gao, P.; Zheng, H.; Wang, K. A Comprehensive Research on

Internal Short Circuits Caused by Copper Particle Contaminants on Cathode in Lithium-Ion Batteries. *eTransportation* **2022**, *13*, 100183.
(18) Kasnatscheew, J.; Börner, M.; Streipert, B.; Meister, P.; Wagner, R.; Cekic Laskovic, I.; Winter, M. Lithium Ion Battery Cells under Abusive Discharge Conditions: Electrode Potential Development and Interactions between Positive and Negative Electrode. *J. Power Sources* **2017**, *362*, 278−282.
(19) Sa, Q.; Heelan, J. A.; Lu, Y.; Apelian, D.; Wang, Y. Copper Impurity Effects on $LiNi_{1/3}Mn_{1/3}Co_{1/3}O_2$ Cathode Material. *ACS Appl. Mater. & Interfaces* **2015**, *7* (37), 20585−20590.
(20) Zhao, M.; Dewald, H. D.; Staniewicz, R. J. Quantitation of the Dissolution of the Graphite-Coated Copper Foil in Lithium-Ion Battery Electrolytes by Flame Atomic Absorption Spectroscopy. *Electrochim. Acta* **2004**, *49* (5), 677−681.
(21) Langner, T.; Sieber, T.; Acker, J. Studies on the Deposition of Copper in Lithium-Ion Batteries during the Deep Discharge Process. *Sci. Rep.* **2021**, *11* (1), 6316.
(22) Diaz, L. A.; Strauss, M. L.; Adhikari, B.; Klaehn, J. R.; McNally, J. S.; Lister, T. E. Electrochemical-Assisted Leaching of Active Materials from Lithium Ion Batteries. *Resour. Conserv. Recycl.* **2020**, *161*, 104900.
(23) Peng, F.; Mu, D.; Li, R.; Liu, Y.; Ji, Y.; Dai, C.; Ding, F. Impurity Removal with Highly Selective and Efficient Methods and the Recycling of Transition Metals from Spent Lithium-Ion Batteries. *RSC Adv.* **2019**, *9* (38), 21922−21930.
(24) Merkoci, A.; Vasjari, M.; Fabregas, E.; Alegret, S. Determination of Pb and Cu by Anodic Stripping Voltammetry Using Glassy Carbon Electrodes Modified with Mercury or Mercury-Nafion Films. *Microchim. Acta* **2000**, *135* (1−2), 29−33.
(25) Landy, M. P. An Evaluation of Differential Pulse Anodic Stripping Voltammetry at a Rotating Glassy Carbon Electrode for the Determination of Cadmium, Copper, Lead and Zinc in Antarctic Snow Samples. *Anal. Chimc Acta* **1980**, *121*, 39−49.
(26) Buldini, P. L.; Saxena, P.; Saxena, V.; Toponi, A. Voltammetric Determination of Trace Amounts of Copper, Cadmium and Lead in Lead-Acid Battery Electrolyte. *Analyst* **1990**, *115* (8), 1073.
(27) de Oliveira, M. F.; Saczk, A. A.; Okumura, L. L.; Fernandes, A. P.; de Moraes, M.; Stradiotto, N. R. Simultaneous Determination of Zinc, Copper, Lead, and Cadmium in Fuel Ethanol by Anodic Stripping Voltammetry Using a Glassy Carbon-Mercury-Film Electrode. *Anal. Bioanal. Chem.* **2004**, *380* (1), 135−140.
(28) Kiekens, P.; Mertens, M.; Bogaert, M.; Temmerman, E. Determination of Mercury by Anodic-Stripping Voltammetry Using a Glassy Carbon Rotating Disc Electrode. *Analyst* **1984**, *109* (7), 909.
(29) Wygant, B. R.; Lambert, T. N. Thin Film Electrodes for Anodic Stripping Voltammetry: A Mini-Review. *Front. Chem.* **2021**, *9*, 809535.
(30) Kokkinos, C.; Economou, A. Stripping Analysis at Bismuth-Based Electrodes. *Curr. Anal. Chem.* **2008**, *4* (3), 183−190.
(31) Barón-Jaimez, J.; Joya, M. R.; Barba-Ortega, J. Bismuth Electrodes, an Alternative in Stripping Voltammetry. *J. Phys. Conf.* **2013**, *466*, 012025.
(32) Economou, A. Bismuth-Film Electrodes: Recent Developments and Potentialities for Electroanalysis. *TrAC, Trends Anal. Chem.* **2005**, *24* (4), 334−340.
(33) Wang, J.; Lu, J.; Kirgöz, Ü. A.; Hocevar, S. B.; Ogorevc, B. Insights into the Anodic Stripping Voltammetric Behavior of Bismuth Film Electrodes. *Anal. Chim. Acta* **2001**, *434* (1), 29−34.
(34) Baldo, M. A.; Daniele, S. Anodic Stripping Voltammetry at Bismuth-coated and Uncoated Carbon Microdisk Electrodes: Application to Trace Metals Analysis in Food Samples. *Anal. Lett.* **2004**, *37* (5), 995−1011.
(35) Prior, C.; Lenehan, C. E.; Walker, G. S. Enhanced Resolution of Copper and Bismuth by Addition of Gallium in Anodic Stripping Voltammetry with the Bismuth Film Electrode. *Electroanalysis* **2006**, *18* (24), 2486−2489.
(36) Prior, C.; Lenehan, C. E.; Walker, G. S. Utilising Gallium for Enhanced Electrochemical Copper Analysis at the Bismuth Film Electrode. *Anal. Chim. Acta* **2007**, *598* (1), 65−73.
(37) Pacheco, W. F.; Miguel, E. M.; Ramos, G. V.; Cardoso, C. E.; Farias, P. A. M.; Aucélio, R. Q. Use of Hydrogen Peroxide to Achieve Interference-Free Stripping Voltammetric Determination of Copper at the Bismuth-Film Electrode. *Anal. Chim. Acta* **2008**, *625* (1), 22−27.
(38) Anastasiadou, Z. D.; Sipaki, I.; Jannakoudakis, P. D.; Girousi, S. T. Square-Wave Anodic Stripping Voltammetry (SWASV) for the Determination of Ecotoxic Metals, Using a Bismuth-Film Electrode. *Anal. Lett.* **2011**, *44* (5), 761−777.
(39) Bobrowski, A.; Królicka, A.; Śliwa, J.; Zarębski, J. Electrochemical Sensing of Copper Employing Tellurium Film Electrode. *Electrochim. Acta* **2017**, *252*, 453−460.
(40) Bobrowski, A.; Królicka, A.; Śliwa, J.; Zarębski, J.; Economou, A.; Kalcher, K. Tellurium Film Electrodes Deposited on Carbon and Mesoporous Carbon Screen-printed Substrates for Anodic Stripping Voltammetric Determination of Copper. *Electroanalysis* **2018**, *30* (9), 2004−2010.
(41) Nagaosa, Y.; Zong, P.; Kamio, A. Selenium-Coated Carbon Electrode for Anodic Stripping Voltammetric Determination of Copper(Ii). *Microchim. Acta* **2009**, *167* (3−4), 241−246.
(42) Tian, Y. Q.; Luo, H. Q.; Li, N. B. Stannum Film Electrode for Square Wave Voltammetric Determination of Trace Copper(Ii). *J. Solid State Electrochem.* **2012**, *16* (2), 529−533.
(43) Sosa, V.; Barceló, C.; Serrano, N.; Ariño, C.; Díaz-Cruz, J. M.; Esteban, M. Antimony Film Screen-Printed Carbon Electrode for Stripping Analysis of CD(II), Pb(Ii), and Cu(Ii) in Natural Samples. *Anal. Chim. Acta* **2015**, *855*, 34−40.
(44) Dastangoo, H.; Majidi, M. R.; Kalantar Hormozi, M. Stripping Voltammetry on Palladized Aluminum: A Novel Sensing Platform for Trace Analysis of Copper. *Microchem. J.* **2023**, *187*, 108404.
(45) Cpsta, B. The Underpotential Electrodeposition of Copper on Polycrystalline Rhodium. *J. Electroanal. Chem.* **1983**, *145* (1), 189−199.
(46) Salgado, L.; Sánchez, H.; Cabrera, C. R.; Castro, R. J.; Meas, Y. Underpotential Deposition of Cu on Partially Oxidized Rh Electrodes. *J. Solid State Electr.* **1998**, *2* (6), 405−412.
(47) Anjos, D. M.; Rigsby, M. A.; Wieckowski, A. Underpotential Deposition of Copper and Silver on Single Crystal Surfaces of Rhodium. *J. Electroanal. Chem.* **2010**, *639* (1−2), 8−14.
(48) Wardak, C.; Pietrzak, K.; Grabarczyk, M. Ionic Liquid-Multiwalled Carbon Nanotubes Nanocomposite Based All Solid State Ion-Selective Electrode for the Determination of Copper in Water Samples. *Water* **2021**, *13* (20), 2869.
(49) Fan, Y.; Xu, C.; Wang, R.; Hu, G.; Miao, J.; Hai, K.; Lin, C. Determination of Copper(Ii) Ion in Food Using an Ionic Liquids-Carbon Nanotubes-Based Ion-Selective Electrode. *J. Food Compos. Anal.* **2017**, *62*, 63−68.
(50) Ghaedi, M.; Montazerozohori, M.; Sahraei, R. Comparison of the Influence of Nanomaterials on Response Properties of Copper Selective Electrodes. *J. Ind. Eng. Chem.* **2013**, *19* (4), 1356−1364.
(51) Yang, C.; Zheng, M.; Qu, R.; Zhang, H.; Yin, L.; Hu, W.; Han, J.; Lu, J.; You, Y. Engineering a Boron-rich Interphase with Nonflammable Electrolyte toward Stable Li||NCM811 Cells under Elevated Temperature. *Adv. Mater.* **2024**, *36* (1), 2307220.
(52) Wu, H.; Zhou, X.; Yang, C.; Xu, D.; Zhu, Y.-H.; Zhou, T.; Xin, S.; You, Y. Concentration-Gradient Nb-Doping in a Single-Crystal $LiNi_{0.83}Co_{0.12}Mn_{0.05}O_2$ Cathode for High-Rate and Long-Cycle Lithium-Ion Batteries. *ACS Appl. Mater. Interfaces* **2023**, *15* (15), 18828−18835.

https://doi.org/10.1021/jacsau.4c01159
JACS Au 2025, 5, 1060−1068